International Journal of Science and Research (IJSR)
ISSN: 2319-7064
SJIF (2020): 7.803

How Would We Know if We Were Living in a Multiverse?

Avni Bansal

The International School Bangalore
bavni[at]tisb.ac.in

Abstract: ***This paper reviews two studies that deal with the simulation of false vacuum bubble collisions and decay, and proposes that searching for evidence of particle scattering outcomes that would result from false vacuum bubble collisions in the CMBR could support the inflationary multiverse hypothesis.***

Keywords: Inflation, Multiverse, False Vacuum, Particle Scattering, CMBR

1. Introduction

Many multiverse theories have been proposed, but very few make testable predictions verifiable with existing technology. The inflationary multiverse hypothesis is amongst this testable minority. According to this hypothesis, space is dotted with an infinity of independent bubble universes. Our universe is one such bubble. If our bubble has collided with another universe bubble in the past, the collision may have left detectable signatures.

This paper discusses how cosmologists are using various techniques to determine the signatures left behind by bubble collisions. In particular, cosmologists are working on two different ways to simulate bubble collisions: classical computer simulations and quantum annealer simulations (Wood, 2021).

Signatures are most likely to take the shape of specific patterns in the Cosmic Microwave Background Radiation (CMBR) and certain types of gravitational waves. Most current research focuses on determining the precise nature of these CMBR patterns and gravitational waves. Once this is done, the signatures can be searched for with instruments like detectors at the Laser Interferometer Gravitational-Wave Observatory (LIGO) and telescope systems like the CMB-S4.

2. Literature Survey

A popular multiverse theory is the chaotic eternal inflation multiverse theory. This stems from the theory of cosmological inflation: the theory that the early universe expanded by a factor of at least 10^{78} within a fraction of a second. After the inflationary epoch, the universe continued to expand but at a much slower rate.

One extension of the theory of cosmological inflation is chaotic eternal inflation. According to the chaotic eternal inflationary theory, the exponential expansion of space never completely stopped. Although our bubble of the universe has slowed down and stopped inflating, eternal inflation tells us that there must always be some other pockets of the universe that are still inflating.

According to chaotic inflation theory, the universe consists of swathes of inflating space interspersed with non-inflating bubble universes like our own. Inflation is also continually coming to a stop in some inflating regions, birthing new bubble universes. This is the chaotic eternal inflation multiverse theory.

The most compelling evidence for the inflationary multiverse would be if another bubble universe were to collide with our own. Such a collision would leave a very specific signature in something called the Cosmic Microwave Background (CMB). The CMB is electromagnetic radiation that originated in the very early universe. Since this radiation is nearly as old as our universe, if our universe originated due to a collision between two bubbles, the collision must have left an imprint on the CMB (see figure 1). The nature of this imprint could be determined through computer simulation models and detected using radio telescopes.

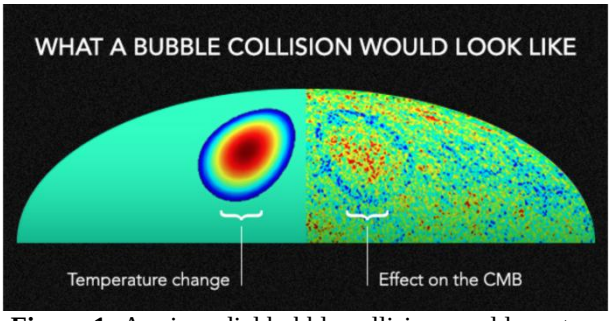

Figure 1: A primordial bubble collision would create a different temperature patch in the otherwise largely isotropic CMB (S. M. Feeney et al., 2011, p. 3)

The CMB-S4 will be the most sensitive CMB detection system in the world. It will consist of a network of extremely sensitive ground-based telescopes deployed at the South Pole and the Atacama Plateau in Chile. One of its goals will be to search for primordial gravitational waves and other evidence of inflation. Since the CMB-S4 will be an order of magnitude more sensitive than previous ground-based telescopes, the data it gathers about inflation will help refine inflationary multiverse models.

A bubble collision may also create gravitational waves. Gravitational waves are essentially ripples in spacetime. These ripples are created when huge masses are accelerated, such as when two massive black holes or neutron stars collide (see figure 2). Computer simulations can determine the nature of the gravitational waves produced when two universes collide.

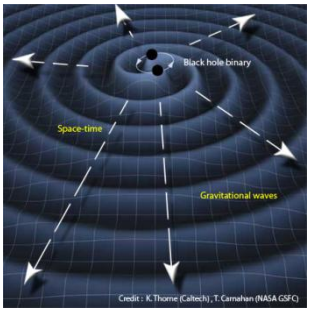

Figure 2: Black hole collision generating gravitational waves (Moskovitz, 2009, p. 1).

In addition to the CMB-S4, LIGO can also be used to detect gravitational waves. There are two LIGO observatories. One is at Haverford Site, Washington, and the other is 3000 km away in Livingston, Louisiana. Each observatory has two mirrors spaced four km apart. The mirrors can detect the small perturbations caused by a gravitational wave. The distance between the observatories creates a delay between when the gravitational waves reach the first observatory and the second. The delay is used to pinpoint the gravitational wave source.

One theory posits that inflation can begin due to something called false vacuum decay. A false vacuum is a concept in quantum field theory. Space is in a false vacuum state when it takes on a local minimum energy value of a field. In contrast, a true vacuum state occurs at the global minimum energy value of a field. Random quantum fluctuations can cause a false vacuum state to undergo a false vacuum decay, lose energy, and settle into a true vacuum. The energy lost during false vacuum decay makes the true vacuum bubble balloon outward. In other words, the bubble inflates. Thus, one popular approach to simulating colliding bubble universes has been to create models of vacuum bubbles.

Classical Computer Approach

Researchers created a simplified simulation to understand the signatures produced by bubble universe collisions (Ashley et al., 2021, p. 1). Each false vacuum bubble was represented as a meson, and each meson contained a kink particle and an antikink particle. Due to wave-particle duality, kink and antikink particles can also be represented as waves called solitons. Solitons can self-propagate while retaining their shape and velocity. They are apt models for bubble collisions because the way a soliton self-propagates is similar to the way a bubble universe inflates.

When the kink and antikink solitons collide, there are three possible outcomes (figure 3(a), (b), (c)): free collisions in which the solitons do not interact (a), elastic collisions in which they do interact but do not produce new particles (b), and inelastic collisions in which they interact and produce new particles (c). When new particles are produced, radiation may be emitted. Thus, the simulation could reveal what kinds of radiation to search for in the CMB.

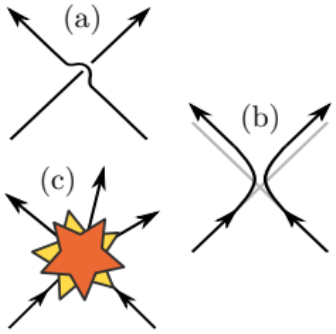

Figure 3: Kink-antikink collision outcomes (Ashley et al., 2021, p. 2)

The physics of bubble collisions was described using a lattice Quantum Field Theory (QFT) (see figure 4), a theory defined on a discrete spacetime lattice instead of being defined continuously. This simulation included just above 1,000 lattice points. The QFT lattice was modeled with a mathematical entity called an extended transverse-field Ising quantum spin chain (H, see equation 1). Ising chains are statistical models used to describe phase changes, such as the phase change from a false vacuum to a true vacuum.

Figure 4: Quantum Field Theory 1+1 D Lattice (Hauke et al., 2013, p.2)

$$H = \sum_{j=1}^{N} \left[-Z_j Z_{j+1} - gX_j - hZ_j + \lambda \left(X_j Z_{j+1} Z_{j+2} + Z_j Z_{j+1} X_{j+2} \right) \right], \quad (1)$$

Equation 1: The extended transverse-field Ising quantum spin chain (Ashley et al., 2021, p. 3)

The above equation is a generic Ising quantum spin chain. It has three adjustable parameters. Here, g is the acceleration due to gravity, h is the value of a symmetry-breaking field, λ is the parameter that controls whether the spin chain is integrable, Z is the magnetization, N is the number of lattice points, and X is the position of the lattice. If the kink-antikink collision is to be inelastic, then H must be non-integrable, so λ was set accordingly. The value of g was set to a small non-zero value because when H is minimized for a small value of g, then H settles into a metastable false vacuum instead of a true vacuum. The value of h must be set to a non-zero value because it is responsible for exerting the force on the kink and antikink that causes them to accelerate and collide.

After constructing the lattice with the Ising chain, the next step was to construct the vacuum bubble. The kink and antikink states inside the vacuum bubble were constructed using Matrix Product States. A Matrix Product State is the quantum state of multiple particles in a system, and it can be represented as a tensor network. A false vacuum and a true

vacuum can both be represented using a chain of known tensors.

Let  be a true vacuum tensor and  be a false vacuum tensor. The energy released due to a kink-antikink collision allows the false vacuum to decay into a true vacuum, so the kink and antikink can be thought of as bridges connecting the true vacuum and the false vacuum. Thus, the kink and antikink states can be constructed by inserting the tensors  (kink) and  (antikink), respectively, between the true vacuum and false vacuum tensor chains. The energy functions of the kink and antikink can be found from H. The tensors  and  are found by minimizing these energy functions. After the kink and antikink Matrix Product States are constructed (see figure 5), they are combined to create the entire vacuum bubble, which is represented by the wave function (ψ, see equation 2). In this equation, the j subscript represents a kink, and the k subscript an antikink. The function f gives the quasiparticle wave packets of the kink (L) or antikink (R) as a function of its position (x) and momentum (p), and $\kappa\overline{\kappa}_{jk}$ is the combined matrix product state of a kink-antikink pair.

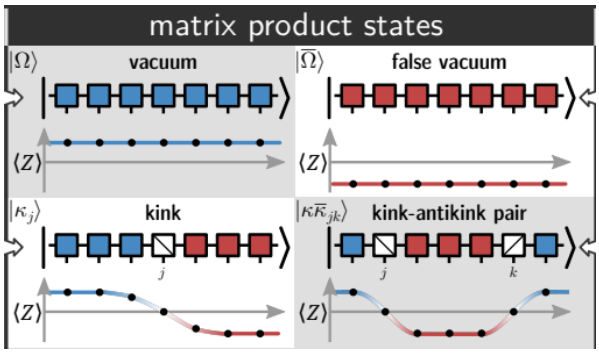

Figure 5: Tensor diagram for true vacuum, false vacuum, kink, and kink-antikink Matrix Product States (Ashley et al., 2021, p. 5)

$$|\Psi\rangle = \sum_{j<k} f_j(x_L, p_L) f_k(x_R, p_R) |\kappa\overline{\kappa}_{jk}\rangle \quad (2)$$

Equation 2: The wave function of the vacuum bubble (Ashley et al., 2021, p. 5)

The researchers also defined a subspace spanned by all the basis states in the vacuum bubble wave function. This subspace can be called sector 1 (see figure 6). Once the vacuum bubble and subspace were defined, the vacuum bubble collision was simulated by using numerical integration to make the wave function evolve in sector 1. As the wave function evolved, the researchers tracked the spin, energy, and entanglement of the system. New particles are produced as entanglement increases when the kink and antikink interact. Hence, entanglement is used as a proxy for particle production: the greater the entanglement, the greater the likelihood of particle production. Secondly, if the collision produces new mesons, the mesons will spread ballistically because they are not affected by the h force field. Thus, a ballistic energy spread would imply meson creation. Thirdly, if the part of the wave function in sector 1 decreases over time, this is another indication of particle creation because it means that energy is leaking away and being utilized in particle production.

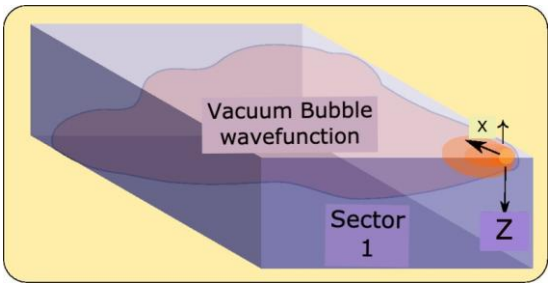

Figure 6: The vacuum bubble wave function situated in Sector 1 (author-generated)

$E_k(p)$ is the kink or antikink dispersion relation, and it expresses energy as a function of momentum. In the QFT being used, the momentum of the quantum field p was bounded ($-\pi \leq p \leq \pi$). The velocity at which the vacuum bubble inflates is the rate of change $\left(\frac{\partial E_k(p)}{\partial p}\right)$ of $E_k(p)$ with respect to p. Since $E_k(p)$ was bounded, the velocity was also bounded. This meant that once the vacuum bubble reached its maximum velocity, its velocity would start decreasing again until the bubble resumed its initial momentum and position. Then it would start inflating again. This is a Bloch oscillation (see figure 7). Since Bloch oscillations cause inflation to reverse once the lattice reaches a certain peak velocity, the researchers could not simulate high-speed, high-energy collisions.

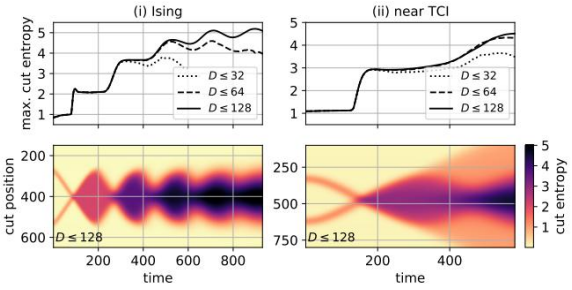

Figure 7: In figure (i), $h = 0$ and $\lambda = 0$ and Bloch oscillations occur, so the bubble position changes periodically. In figure (ii), $\lambda > 0$, so the bubble inflates and spreads outwards (Ashley et al., 2021, p. 9)

Inflation occurs when false vacuum potential energy is converted into kinetic energy. The larger the false vacuum bubble, the greater its potential energy, and thus the faster it expands. In order to avoid Bloch oscillations, the λ, h, and g parameters in H were kept small, as small values lead to small bubble sizes.

Classical Computer Results

When the simulation was run with λ and h set to zero, no evidence of inelastic collisions was found. Even when the collision energy was set much higher than the energy required for meson production, no ballistic energy spread was recorded. Post-collision, the probability that parts of the wave function had left sector 1 was 10^{-5}. Thus, when there is

no symmetry-breaking force field, vacuum bubbles are stable and only undergo elastic collisions.

When λ was made non-zero, evidence of inelastic collisions appeared. Ballistic energy spread was observed, implying meson creation. The probabilities of various particle scattering outcomes were also computed (see figure 8). The mesons in each scattering outcome contribute *EP* energy to the lattice, where *E* is the total energy of the lattice and P is the probability of that scattering outcome. E_{pkts} is the total excess energy due to particle production in the region of the lattice containing the ballistically expanding meson. *E* and E_{pkts} can be measured from the simulations. Then, $EP = E_{pkts}$ can be used to calculate scattering outcome probabilities. Four major scattering outcomes were found, having probabilities 62%, 19%, 7% and 7%.

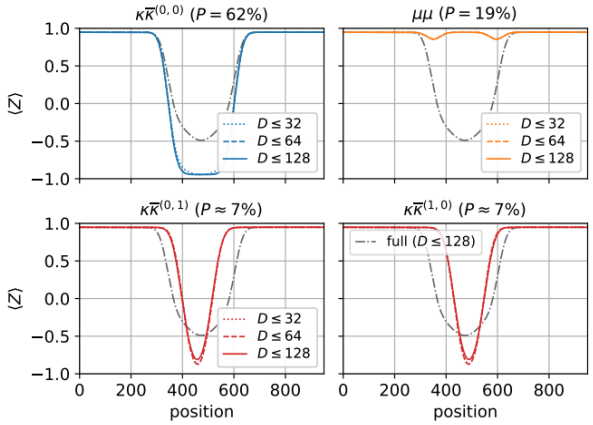

Figure 8: High probability scattering outcomes. Here, Z represents the spin values of the wave function. Negative spin values indicate that the wave function is outside Sector 1 (Ashley et al., 2021, p. 9)

Quantum Annealer Approach

Indeed, another study has developed a mathematical approach for simulating any QFT on a quantum annealer, which is a type of quantum computer. Specifically, a quantum annealer is an optimization device that leverages quantum fluctuations to find the minimum value of a function. The study invented a method for encoding any QFTs into the annealer and running minimization experiments on them. Since a false vacuum decay is a transition from a local energy minimum in a field to a global energy minimum, the quantum annealer could be used to simulate the false vacuum decay of an inflationary field.

To vet the mathematical approach, the study's authors did, in fact, simulate the false vacuum decay of a QFT. Then, they compared the observations from the simulation with theoretical predictions. In order to run the experiment, an arbitrary quantum field (ϕ) was chosen, and its potential energy function ($U(\phi)$) was constructed (see Equation 3).

$$U(\phi) = \frac{3}{4}\tanh^2\phi - k(t)\,\mathrm{sech}^2\left(c(\phi - v)\right) \quad (3)$$

Equation 3: The potential energy of the quantum field as a function of the value of the quantum field (Steven et al., 2021, p. 2)

In Equation 3, the $\frac{3}{4}tanh^2(\phi)$ term creates a potential energy well (see figure 9), which represents the false vacuum. The $\frac{3}{4}sech^2(c(\phi - v)$ term creates a second potential energy well. The v parameter is the vacuum displacement between the first energy well and the second. The k term is the coupling parameter. When k is initially zero, there is only one energy well corresponding to the false vacuum, so the annealer settles into the false energy potential well. As k is gradually turned on, the second energy well starts growing deeper until it is deeper than the false vacuum well. Since the second well becomes the lowest-energy value of the field, it is effectively the field's true vacuum.

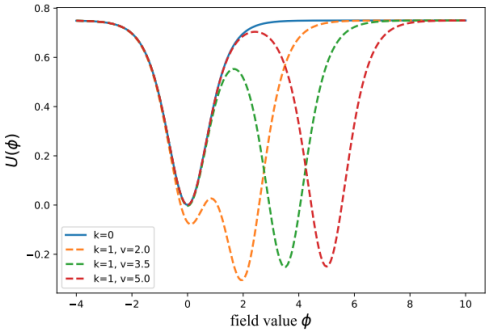

Figure 9: Graph of $U(\phi)$ for different values of k. When k is zero, there is only one energy well, and when k is non-zero, there are two wells (Steven et al., 2021, p. 2)

After setting up the annealer, theoretical estimates were made about what would be observed during a false vacuum decay. A Schrodinger equation is a linear partial differential equation that represents the wave function of a quantum mechanical system. Since $U(\phi)$ represents the potential energy state of a quantum field system, it can be thought of as a Schrodinger equation. A path integral is the sum of all possible paths taken through spacetime. A worldline of an object is the path an object takes through spacetime. The most likely path taken from the false vacuum to the true vacuum is the worldline path integral of $U(\phi)$ (see Equation 4.).

$$\langle \eta_i | \eta_f \rangle = \int_{\eta(0)=\eta_i}^{\eta(T)=\eta_f} \mathcal{D}\eta\, e^{-i\hbar^{-1}\int_0^T dt\left(\frac{1}{2}m\dot{\eta}^2 - (U - E_0)\right)}, \quad (4)$$

Equation 4: The worldline path integral of $U(\phi)$ with limits from the false vacuum to the true vacuum.

Here, time is T, the variable of integration is D, m is the starting scalar value of the field, E_o is the true vacuum energy minimum, and η gives the position of the field as a function of time.

Next, the path integral is used to evaluate the steepest decay rate of $U(\phi)$. At the point of steepest descent, the path integral behaves classically rather than quantum

mechanically, so it can be solved using standard Euclidean mathematical techniques (see Equation 5).

$$\langle \eta_i | \eta_f \rangle_E = \int \mathcal{D}\delta\eta\, e^{-\hbar^{-1}\int dt\left(\frac{m(\dot{\eta}_{cl}+\delta\dot{\eta})^2}{2}+U(\eta_{cl}+\delta\eta)-E_0\right)}, \\ = Ae^{-\hbar^{-1}S_{E,cl}}, \quad (5)$$

Equation 5: The worldline path integral of $U(\phi)$ solved to find the point of steepest descent $U(\phi)$(Steven et al., 2021, p. 3)

Here, $S_{E,cl} = \int_{\eta_+}^{\eta_e} d\eta\sqrt{2m(U-E_0)}$, where η_e and η_+ represent two positions of the field when it is undergoing its steepest decay.

The decay rate during the steepest descent is $\Gamma = |\langle \eta_i | \eta_f \rangle_E|^2$. Evaluating this, Γ comes out to be:

$$\Gamma \approx e^{-2\hbar^{-1}S_{E,cl}} \quad (6)$$

Equation 6: The decay rate of $U(\phi)$ at the point of steepest descent. $S_{E,cl}$ is an expression that depends on the vacuum separation (v). (Steven et al., 2021, p. 3)

Once the decay rate has been theoretically calculated, the annealer is run, and the experimental decay rate is measured. In order to run the experiment, the annealer is set up to model the QFT. The annealer is represented by an Ising model of the form:

$$\mathcal{H}_{QA} = A(s)\left(\sum_{ij}\hat{J}_{ij}\sigma_i^Z\sigma_j^Z + C(t)\sum_i \hat{h}_i\sigma_i^Z\right) \\ + B(s)\sum_i \sigma_i^X, \quad (7)$$

Equation 7: The Ising model of the quantum annealer (Steven et al., 2021, p. 4)

In Equation 7, σ_i and σ_j represented the annealer's qubits. A quantum computer's bits are analogous to a classical computer's bits. The A(s) function consists of terms that represent the classical part of the annealer system, and the B(s) function consists of terms that represent the quantum mechanical part (see figure 10). The s parameter can range from zero to one. At s = 1, A(s) = 1 and B(s) = 0, so the system is purely classical. At s = 0, A(0) = 0 and B(0) = 1, so the system is purely quantum mechanical.

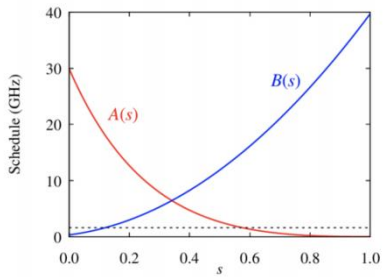

Figure 10: Values of A(s) and B(s) for different values of s (Steven et al., 2021, p. 6)

The h and J terms are as follows:

$$J_{ij}^{(\text{chain})} = -\frac{\Lambda}{2}\begin{pmatrix} 0 & 1 & & & & \\ 1 & 0 & 1 & & & \\ & 1 & 0 & & & \\ & & & \ddots & & \\ & & & & 0 & 1 \\ & & & & 1 & 0 \end{pmatrix}, \\ h^{(\text{chain})} = \Lambda'\,(1,0,0\ldots,0,-1), \quad (8)$$

Equation 8: The J and h terms in the Ising model of the annealer (Steven et al., 2021, p. 4)

The value of the QFT can be determined by the annealer at the position where a quantum spin-flip occurs. The h array forces the QFT in the annealer to have a quantum spin of +1 on one side and -1 on the other side. The J matrix forces the QFT to have as few spin flips from positive to negative or vice versa as possible. Consequently, there is only one position where a quantum flip occurs. The annealer uses this position to find the QFT's value.

After setting up the QFT on the annealer, $U(\phi)$ is encoded. The potential is first split into two parts, U_0 and U_1 (see Equation 9), where U_0 corresponds to the false vacuum well and $U(1)$ corresponds to the true vacuum well. Initially, the coefficient of U_1 (k) is kept zero, so $U(\phi) = U_0$, and the annealer settles to a false vacuum. Later, k is turned on so that the true vacuum appears. The split $U(\phi)$ is encoded into the annealer by adding some extra terms called couplings to J and h.

$$U_0 = \frac{3}{4}\tanh^2\phi, \;;\; U_1 = -k(t)\text{sech}^2(\phi - v), \quad (9)$$

Equation 9: Splitting U into two segments (Steven et al., 2021, p. 5)

Once $U(\phi)$ is encoded, an anneal routine is devised. The anneal routine depends on how the s parameter in A(s) and B(s) varies over time. In a forward anneal, s will be initialized to a value close to zero so the system is highly quantum. Then s will be incrementally lowered to zero so that the system settles into a stable classical state. Conversely, a reverse anneal starts by setting s close to one. Then s is lowered for some interval of time so that quantum mechanical behavior occurs. Lastly, s is raised to one again so the system again settles into a stable classical state. Since this study needed to initialize the annealer in a quasi-stable false vacuum state, a reverse anneal was chosen because it begins in a stable classical state. An h-gain schedule refers to the schedule for turning on k over time. Since a reverse anneal is being conducted, k will initially be incremented slowly, so the system slowly evolves from classical to quantum. Once the system settles into a false vacuum, k is incremented faster to induce false vacuum decay (see Figure 11).

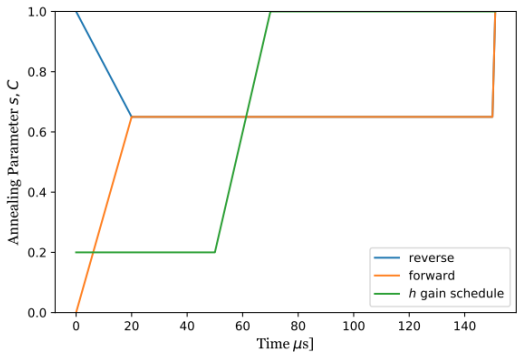

Figure 11: Variations in s for a forward anneal and reverse anneal, and the h gain schedule for a reverse anneal (Steven et al., 2021, p. 6)

Quantum Annealer Results

When the reverse anneal was done with s ranging from 0.7 to 1, the log of the decay rate was found to be $\log \Gamma = 2.29 \times (1.71 - v)$, while the theoretically predicted value was $\log \Gamma = 3.0 \times (1.66 - v)$. The result is within the bounds of experimental uncertainty. Another theoretical prediction was that the decay rate would be suppressed exponentially as v increases. This was also observed experimentally (see figure 12.)

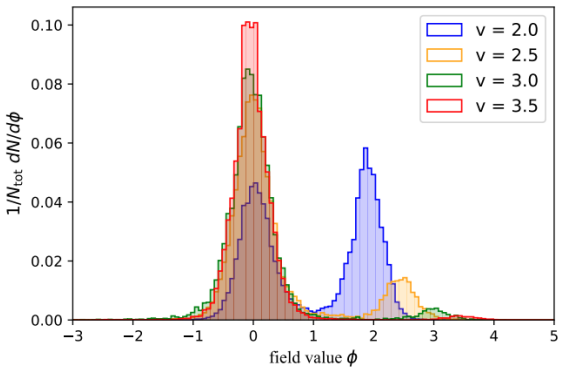

Figure 12: Exponential suppression of decay rate as v increases (Steven et al., 2021, p. 8)

3. Conclusion

Using a classical computer simulation where vacuum bubbles were modelled as mesons, it was determined that kink-antikink collisions are inelastic when the spin chain integrability parameter is non-zero. Furthermore 4 high probability particle scattering outcomes from the inelastic kink-antikink collisions were computed.

In a second study, a quantum annealer was set to a false vacuum and allowed to decay into a true vacuum. The decay rate was suppressed exponentially as the vacuum displacement between the energy wells increased, which is in agreement with theoretical predictions, and thus increases confidence in existing models of false vacuum decay theory.

4. Future Scope

The high probability scattering outcomes from the classical computer simulation may be detectable with the sensitive instruments of the CMB-S4. Although the Atacama Cosmology Telescope in Cerro Tolo, Chile, has less sensitive instruments, it is also currently searching for bubble collision signatures in the CMB.

Although this study yielded testable predictions about particle scattering signatures in the CMB, it has some limitations. Firstly, only about 1,000 lattice points were considered in the simulation. Since the universe is much larger than 1,000 lattice points, this is an oversimplification. In more complex simulations involving more particles and lattice points, it is possible that new scattering outcomes will become more prominent than the ones found in this study.

Secondly, the study only examined low-speed, low-energy collisions because of the onset of Bloch oscillations. However, our universe may have been formed in a high-energy collision. Thus, it would be instructive to run the simulation with a different QFT, one that allows higher lattice velocities before the onset of Bloch oscillations.

Thirdly, the number of particles and the bubble velocities were constrained due to entanglement. The higher the bubble velocity and the greater the number of collisions between particles, the higher the entanglement. Furthermore, this entanglement grows exponentially. If there are too many particles in the simulation or if the bubbles are moving too fast, then entanglement grows so much that a classical computer cannot simulate it. However, quantum computers are inherently suited to simulating entanglement, so they would make optimal candidates for future bubble collision simulations.

The quantum annealer simulation revealed that the decay rate of a false vacuum varies exponentially with vaccum displacement, in agreement with theoretical predictions. The agreement between theoretical predictions and experimental observations has verified that the quantum annealer simulation approach works. This approach makes it possible to simulate high energy, high speed, many-particle systems without being hindered by the effects of quantum entanglement and classical computational limits. It thus enables a better understanding of what imprints a bubble collision may have left in the CMB.

However, the quantum annealer approach has the same defect that all quantum computer approaches have: quantum decoherence. A quantum computer's qubits must be in a state of quantum coherence for the computer to work. Factors like temperature and electromagnetic interference can make the qubit states decoherent, which creates inaccuracies in the quantum computer's results. The more the qubits, the faster decoherence occurs. A large number of qubits is needed to simulate complex, realistic bubble universes. Decoherence may make this unfeasible for present-day quantum computers.

References

[1] Abel, S., & Spannowsky, M. (2021). Quantum-Field-Theoretic Simulation Platform for Observing the Fate of the False Vacuum. *PRX Quantum*, *2*(1).
[2] Abrams, N. E., & Primack, J. R. (2012). *The New Universe and the Human Future: How a Shared Cosmology Could Transform the World (The Terry Lectures Series)* (Illustrated ed.). Yale University Press.
[3] Feeney, S. M., Johnson, M. C., Mortlock, D. J., & Peiris, H. V. (2011). First observational tests of eternal inflation: Analysis methods and WMAP 7-year results. *Physical Review D*, *84*(4).
[4] Hauke, P., Marcos, D., Dalmonte, M., & Zoller, P. (2013). Quantum Simulation of a Lattice Schwinger Model in a Chain of Trapped Ions. *Physical Review X*, *3*(4).
[5] Milsted, A., Junyu, L., Preskill, J., & Vidal, G. (2021). Collisions of false-vacuum bubble walls in a quantum spin chain. *Quantum Physics*. Published.
[6] Moskowitz, C. (2009, August 19). *Lack of Gravity Waves Puts Limits on Exotic Cosmology Theories*. Space.Com.
[7] Wood, C. (2021, February 24). *Physicists Study How Universes Might Bubble Up and Collide*. Quanta Magazine.

Author Profile

Avni Bansal is a student at The International School Bangalore. Her primary research interests are astronomy and engineering. In particular, she works on non-rocket launch alternatives. She also likes solving challenging math problems and learning about miscellaneous science and humanities topics. In her free time, she enjoys reading across genres and doing CrossFit.